LASER INTERFEROMETER GRAVITATIONAL WAVE OBSERVATORY
- LIGO -
CALIFORNIA INSTITUTE OF TECHNOLOGY
MASSACHUSETTS INSTITUTE OF TECHNOLOGY

Technical Note	**LIGO-T1300836—x0**	2013/09/26

Sensing and control of a six-DOF maglev-based suspension prototype

Giorgos Mamakoukas,Haixing Miao, Koji Arai, Rana Adhikari

California Institute of Technology
LIGO Project, MS 18-34
Pasadena, CA 91125
Phone (626) 395-2129
Fax (626) 304-9834
E-mail: info@ligo.caltech.edu

Massachusetts Institute of Technology
LIGO Project, Room NW22-295
Cambridge, MA 02139
Phone (617) 253-4824
Fax (617) 253-7014
E-mail: info@ligo.mit.edu

LIGO Hanford Observatory
Route 10, Mile Marker 2
Richland, WA 99352
Phone (509) 372-8106
Fax (509) 372-8137
E-mail: info@ligo.caltech.edu

LIGO Livingston Observatory
19100 LIGO Lane
Livingston, LA 70754
Phone (225) 686-3100
Fax (225) 686-7189
E-mail: info@ligo.caltech.edu

http://www.ligo.caltech.edu/

1 Abstract

Seismic noise is one of the most important low-frequency disturbances that limit the sensitivity of advanced gravitational-wave detectors. For isolation, the usual approach has been the multiple-stage pendulum suspension; here an alternative seismic noise isolation scheme is investigated. This scheme utilizes the symmetry and local extremum of the magnetic force between disk magnets andby incorporating the sensing and feedback control system can in principle achieve stable low-frequency isolation of six degrees of freedom. To test this idea, a prototype has been built and the sensing and control of the setup has been successfully tested.

2 Introduction

2.1 Background

Gravitational waves (GWs) constitute a cutting edge field in physics. Despite having been predicted a long time ago by A. Einstein and modeled thereafter, no gravitational wave has ever been directly observed to this point; the Laser Interferometer Gravitational-Wave Observatory (LIGO) seeks to be the first to do so. The LIGO project involves two Michelson interferometers in Livingston, Louisiana and Hanford, Washington, and uses the properties of space-distortion of GWs to detect them. Specifically, GWs distort space—and time—and so are expected to change the physical length of the Michelson Interferometer arms. When that happens, interference changes occur and, in order to detect even small-amplitude GW, interference changes are normally sought near the dark fringes. Given the distance between the Louisiana and Hanford sites and the speed of GWs, a comparison of data can confirm their presence. Unfortunately, the measurements are confounded with irrelevant background noises.

It is a challenge therefore to isolate disturbances from external sources in order to improve the sensitivity of the LIGO detectors in the lower part of the frequency spectrum. At frequencies below 100 Hz, seismic noise is one of the important disturbance sources and our project aims to investigate one possibility of reducing its effects. To achieve this, the usual applied approach is to implement a low-resonance system. Such systems respond only weakly to higher-than-their-resonance frequency disturbances and, thus, serve as isolation techniques. The typical treatment for low-frequencies isolations has been to use a multiple-stage pendulum type suspension, however we investigate a different approach, that of magnetic levitation, aiming to test whether it can also achieve the desired noise isolation.

2.2 Magnetic Levitation System

In the magnetic levitation (maglev) set-up, the test mass (the interferometers' mirror) hangs from a levitated plate. The plate—on which permanent magnets are attached—is also surrounded by fixed magnets of opposite poles, which create an ambient magnetic field and so exert a magnetic force on the plate. Consequently, the plate feels a magnetic and a DC gravity force, which nearly cancel at equilibrium (the small offset is corrected via feedback

control).
The ultimate goal is for the system to have low natural frequency, or equivalently low rigidity. Using rigidity's definition for the linear degrees of freedom

$$K_i = \frac{\partial F_i}{\partial i},$$

where i=x,y,and z the rigidity is zero near an extremum of the magnetic force; the closer to the extremum of the magnetic force the equilibrium point occurs, the lower the rigidity or resonance frequency of the system. The system's rigidity for the angular degrees of freedom manifests similar behavior:

$$K_j = \frac{\partial I_j}{\partial j},$$

where j=yaw, pitch, and roll rotations and I is the corresponding moment of inertia. For the magnetic levitation setup, it has been shown that there exists an extremum of the magnetic force around which the rigidities of the system are low for all six degrees of freedom. As a result, low-frequency isolation is theoretically possible for this innovative approach.[1]

2.3 Feedback Control

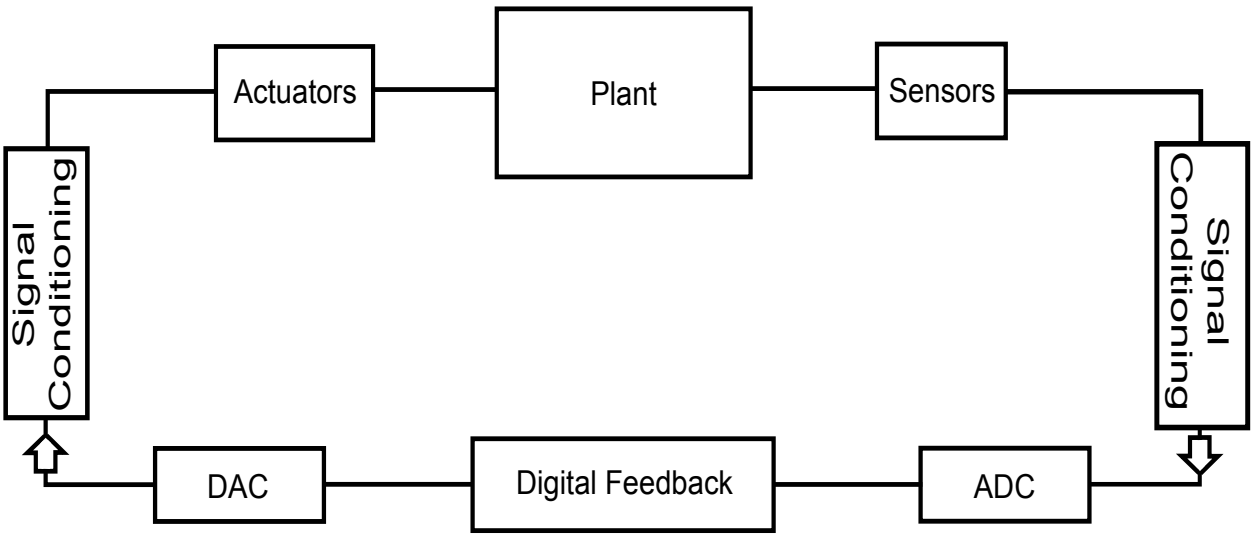

Figure 1: The flow chart shows the closed feedback loop of our system.

However, as explained by Earnshaw's theorem, the maglev configuration is unstable. For this reason, active feedback control with a plant, a sensor, and a controller is used. The plant consists of the levitated plate and the permanent magnets attached to it, whereas the controller behavior is designed by a computer. A start-to-finish procedure of our feedback loop is shown in 1 and is as follows. When the levitated plate (plant) is displaced, the sensors detect changes in the present magnetic field, associated with the plate's movement, and produce a signal. After signal conditioning, the signal is fed—va ADC connections—to a computer, which is used to process the signal and create the appropriate feedback. The signal then is sent, via a DAC connection, to the actuation signal conditioning boards and then reaches the actuators. The latter are control coils wound around the fixed magnets

and the current running through them adjusts the magnetic field around the plate to correct its displacement. For a low-frequency isolation, the ultimate goal remains to achieve low-resonance by moving the equilibrium point near the maximum of the magnetic force. To do so, provide additional, tunable DC offset magnetic field is provided by sending DC current around the fixed magnets . In this way, the equilibrium moves closer to the desired point. In addition to the feedback system, a series of DC motors serve to initially bring the levitated plate within the range of our feedback control.

The performance of each component of the feedback system—plant, sensor and controller—is evaluated with transfer functions, which display the response of the system to a given input over the desired frequency range. Ultimately, the transfer function between the ground motion and the displacement of the levitated plate will give us the actual isolation performance of our configuration. To obtain the transfer function of the plate, either a shaking platform or a sensitive seismometer will be used. The shaking platform produces a vibration (input) on the plate over a frequency spectrum, while at the same time, the displacement (output) of the plate is recorded. Then, plotting the data points yields the transfer function (output/input) of the plate. On the other hand, the seismometer measures the motion of the ground (noise) and the data are fed to a spectrum analyzer, where a Fourier Transform expresses noise as a function of frequency. Ground noise (input signal) along with the data from the plate's displacement (output) determine the plate's transfer function.

Control and sensing in all six degrees of freedom was achieved. Following is a more elaborate description of our progress.

3 Methods

3.1 DC Motors

Before engaging the real-time control, 6 DC motors are used, which are extended or shortened to bring the levitated plate within the range of the feedback control more precisely and conveniently. The range of the feedback control is around the equilibrium, where the net force acting on the plate is small. That means that the farther away from the equilibrium the plate is, the stronger it presses against the motors if it is in contact with them. To use this effect, strain gauge sensors are placed on the side of a copper sheet holder, which is bent when pressed against the plate. The holder so stretches the sensors and increases their electrical resistance, a change that is detected through a Wheatstone Bridge configuration.

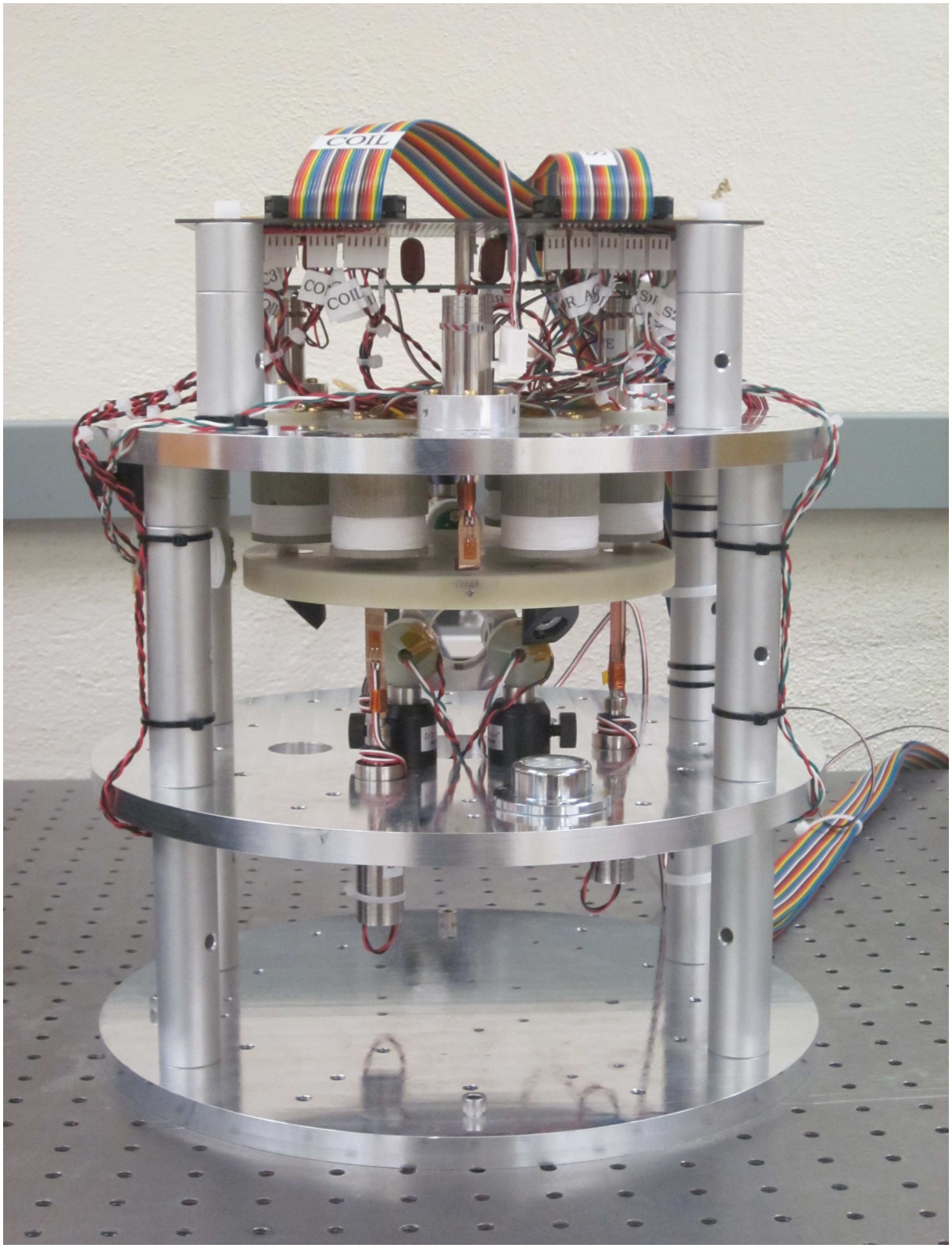

Figure 2: The figure shows the physical setup of our experiment. The plate is surrounded by fixed magnets so that its movement is sensed and a signal is sent to the feedback control. In the picture, one can also see three of the six DC motors (two below and one above the plate).

3.1.1 Wheatstone Bridge and Amplification

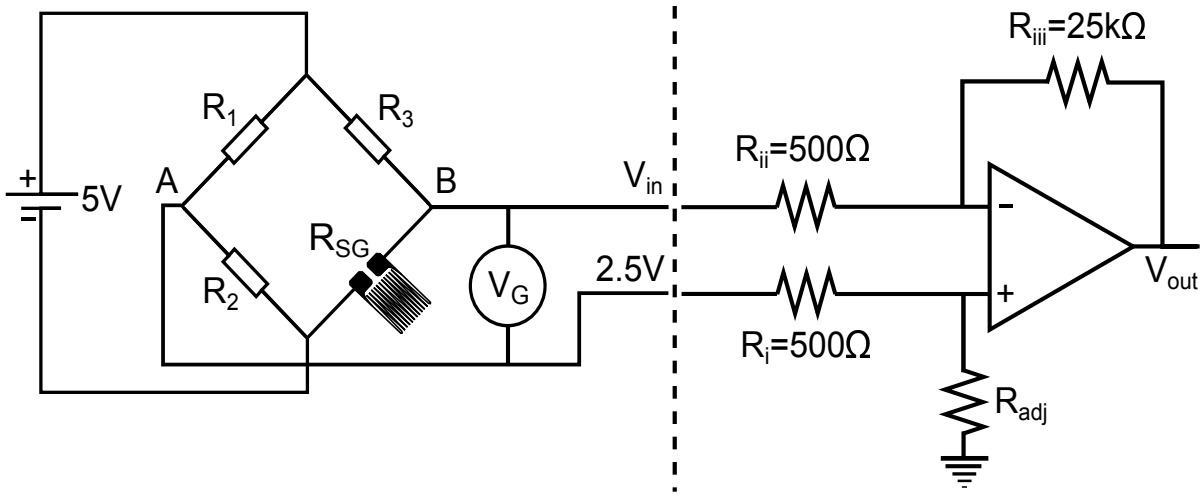

Figure 3: On the left, a typical Wheatstone Bridge circuit; on the right, the amplification circuit. R_{SG} is the resistor of the strain gauge sensor and is around 350Ω. The voltage difference between points A and B is zero when $R_2R_3 = R_1R_{SG}$

The sensors constitute one of the resistors in "balanced" Wheatstone Bridge circuits (see Fig. 3). By "balanced", I mean the voltage difference between points A and B is zero, so that when the plate stretches the sensor and changes its resistance, the Wheatstone bridge circuit creates a signal. To detect even low amplitude signals, we further amplify the voltage offset by connecting the output of the Wheatstone Bridge into an op-amp configuration shown in Fig. 3. For the op-amp circuit, it was calculated that

$$V_{out} = \frac{R_{iii}}{R_{ii}}[V_B - V_A\frac{R_{adj}(R_{ii}R_{iii})}{R_{iii}(R_i + R_{adj})}],$$

where V_A and V_B are the output voltages of the Wheatstone Bridge and $\frac{R_{iii}}{R_{ii}}$ is our gain. For a gain factor of 50, it was chosen $R_{iii} = 25k\Omega$ and $R_{ii} = 500\Omega$ and further $R_{adj} \approx 25k\Omega$ and $R_i = 500\Omega$ such that

$$V_{out} = \frac{R_{iii}}{R_{ii}}(V_B - V_A) \quad (1)$$

and the output of the op-amp is zero whenever there is no voltage difference input from the Wheatstone Bridge. We use digital voltage meters to read the output of each motor on six screens and push the motors up and down according to the offset to bring the levitated plate within the feedback range.

Uncertainties in the resistors' values introduce additional voltage offset to the Wheatstone Bridge even when the strain gauge is not deformed. To best cancel out this inherent voltage offset, we use an adjustable resistor, R_{adj}. The offset needs only be small (a few mV) and not exactly zero, since the DC motors are only used to levitate the plate within the range of the feedback control. At equilibrium, where there will be no force on the sensors, we will read the small voltage offset of the Wheatstone bridge. We tuned the resistors in groups; while the plate was resting against the top motors, we corrected the offset for the bottom ones and vice versa.

To drive the DC motors, we tested different voltage values and chose 5V for a slow-steady pace. To power the motors from our 15V source, we initially used 3.6kΩ resistors in series to the motors, whose internal resistance was measured to be roughly 100Ω. The motors did not move enough, so we replaced the resistors with 1kΩ ones.

Figure 4: The DC motors box with the readouts for the voltage offset (in mV). From left to right, the top readouts correspond to the top motors (TS—top- south—, TW, TE) and the bottom ones to the bottom ones(BN, BS, BE). The red buttons are used to extend the motors and the black ones to shorten them.

In short, when the levitated plate deforms our strain gauge sensors, it effectively increases the resistance in the Wheatstone Bridge, offsetting the voltage difference, which—after fed to our op-amp setup—is reported on a digital voltage meter.

3.2 Sensors

Subsequently, the sensing set-up was prepared. Six Hall-effect sensors are used for sensing six degrees of freedom. Three sensors will be placed coplanar to the levitated plate;one will detect movements on the horizontal y-axis and the other two sensors the angular displacement in the x-y plane (their difference) and the horizontal displacement on the x-axis (their sum). Another three sensors will be above the plate; one will sense vertical displacements (z-axis) and the other two the tilts of the plate.

3.2.1 Hall-effect sensors

For our experiment, Allegro A1323 Hall-effect sensors were used. As is known for the Hall-effect, in the presence of a magnetic field flowing electrons deviate in a specific direction. When enough electrons pile up, they create a measurable electric field, which in turn gives rise to a voltage difference. Hall-effect sensors exploit this idea and simply measure the voltage difference that develops across two plates. Given that voltage reading, one can find the electric field via

$$\mathrm{E} = \frac{\Delta \mathrm{V}}{\mathrm{l}}, \tag{2}$$

where l denotes the separation distance between the plates. Next, the electrostatic force is also known:

$$F = Eq. \tag{3}$$

At equilibrium, the electrostatic force is equal to the magnetic force

$$F_B = q\tilde{v} \times \tilde{B}. \tag{4}$$

Combining 2, 3, 4 we get an expression for the magnetic field strength:

$$B = \frac{\Delta V}{lv}, \tag{5}$$

which subsequently allows to calculate the position of the levitated plate, since the magnets attached on the latter affect the magnetic force felt by the sensors in a determined way. The factor lv depends on the characteristics of the Hall effect sensor and in our case is roughly 2mV/G.[2]
In fact, the present magnetic field is calculated in a different way. Instead of theoretically calculating the magnetic field and the position, the distance of the plate is approximated experimentally. Specifically, the voltage reading of the Hall effect sensors has been recorded for different positions of the Hall effect sensors. The displacement-to-voltage conversion factor is then found by fitting a linear curve to our measurement data points. Throughout the project it became evident that the plate produced too small of a signal to the sensors (roughly 0.193mV/mm), which were for this reason moved closer to the plate. With the new configuration, the sensitivity of the sensors increased roughly by a factor of fifty (≈10 mV/mm).

3.2.2 Voltage Offset

Hall-effect sensors read 2.5V at the presence of no magnetic field. In addition to this inherent offset, the sensors also sense the ambient magnetic field from the fixed magnets. The signal should be zero whenever the plate is at rest and deviate only when the plate is displaced. To correct the voltage offset of the sensors, the op-amp configuration shown in Fig.5 was used. For this configuration, it is true that:

$$V_{in} - V_1 = IR_3 \tag{6}$$

$$V_1 - V_{out} = IR_4 \tag{7}$$

Our voltage source is 5V, so we have also:

$$V_1 = 5\frac{R_2}{R_1 + R_2} \tag{8}$$

Therefore, from equations 6 and 7:

$$V_{in} - V_1 = V_1 - V_{out} \tag{9}$$

Solving for V_{out} and plugging 8, we get:

$$V_{out} = 10\frac{R_2}{R_1 + R_2} - V_{in} \tag{10}$$

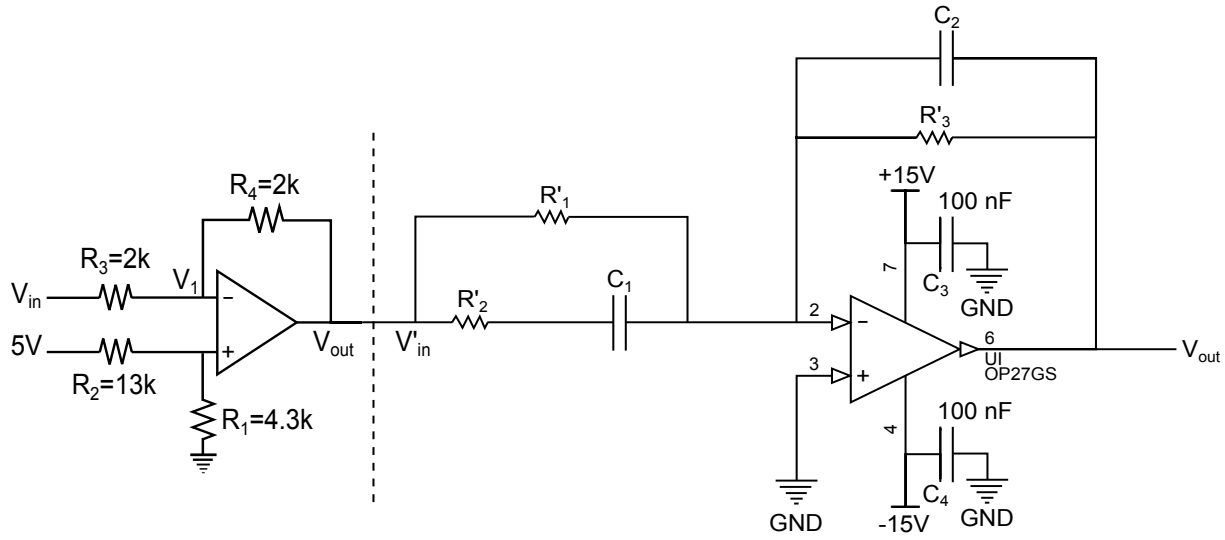

Figure 5: The configuration function in two parts. First, it provides the required voltage offset to ensure a zero signal when the plate is at rest. The voltage divider configuration serves to use our voltage source of 5V and transform it to the required voltage offset for our op-amp Next, it applies a high-pass filter to boost the low-amplitude signal of high-frequency displacement, so that this information is not lost before reaching the digital feedback.

The values of R1 and R2 are determined from the desired voltage offset, which in turn depends on the position of the HE sensors and the corresponding readout. The offset of each HE sensor was measured and the resistors were selected so as to appropriately adjust the voltage offset. The final resistors values for each sensor are shown in Table 1.

Sensors	R1	R2
AC1	110k	2.2k
AC2	130k	2.2k
AC3	62k	1.2k
S1	7.5k	2.2k
S2	20k	7.5k
N	20k	6.2k
E	4.3k	1.5k

Table 1: The resistors used to correct the voltage offset of the HE sensors. Given these resistors, the offset cannot be nullified completely and so the digital system is later used to adjust it.

3.2.3 Whitening

A high-pass filtering was also introduced in the sensors' conditioning circuit (see Fig. 5). As explained already, the levitated plate has—as any system— poor response above its resonance frequency. Small displacements mean small signal and the signal must be amplified such

that high frequency displacements more readily detectable. In principle, the signal should be amplified over the whole range, however the plate has great response below or at its natural frequency and our signal might, in that case, be outside our processable range. At the end, the goal is to acquire an equal amplitude signal over the whole spectrum, a process known as whitening.

The behavior of the configuration shown on the right side of Fig. 5 was calculated to be

$$\frac{V'_{out}}{V'_{in}} = -\frac{R'_1 + R'_2}{R'_1 R'_2 C_2} \frac{s + Z_0}{(s + P_0)(s + P_1)}$$

where

$$Z_0 = \frac{1}{(R'_1 + R'_2)C_1}$$

$$P_0 = \frac{1}{R'_2 C_1}$$

$$P_1 = \frac{1}{R'_3 C_2},$$

where

$$s = i2\pi f$$

and f is the frequency. The variables Z_0, P_0, and P_1 are the zero and the poles of the transfer function respectively, and the coefficient of the function is its gain. For a high-pass filter shape, the zero and two poles must obey this order

$$Z_0 < P_0, P_1.$$

The resonance frequency of the plate was estimated to lie around 2Hz and so this value was chosed to be the zero of the system. After the transfer function of the setup is measured, this value can be redefined to be slightly above the actual natural frequency of the plate. For the other two cut-off values, the first guesses were 50Hz and 200Hz; similarly, these values will be adjusted once the frequency spectrum of the signal is known. The latter values were not precisely derived, but rather estimated so that we amplify signals beyond the resonance frequency. For such cut-off frequencies, the resistors' and capacitors' values were determined: $R'_1 = R'_3 = 13k\Omega$, $R'_2 = 1.5k\Omega$, $C_1 = 2.2\mu F$, $C_2 = 47nF$. These values set the zero and two poles:

$$Z_0 \approx 10\pi rad/s,$$

$$P_0 \approx 96\pi rad/s, \text{and}$$

$$P_1 \approx 520\pi rad/s.$$

The gain of the high-pass filter is

$$\frac{R'_1 + R'_2}{R'_1 R'_2 C_2} \approx 15821$$

and ensures a unity gain at low frequencies.
In the end, the transfer function of the high-pass filter is

$$\frac{V'_{out}}{V'_{in}} \approx |-15821 \frac{s + 31.4}{(s + 301.6)(s + 1633)}|. \tag{11}$$

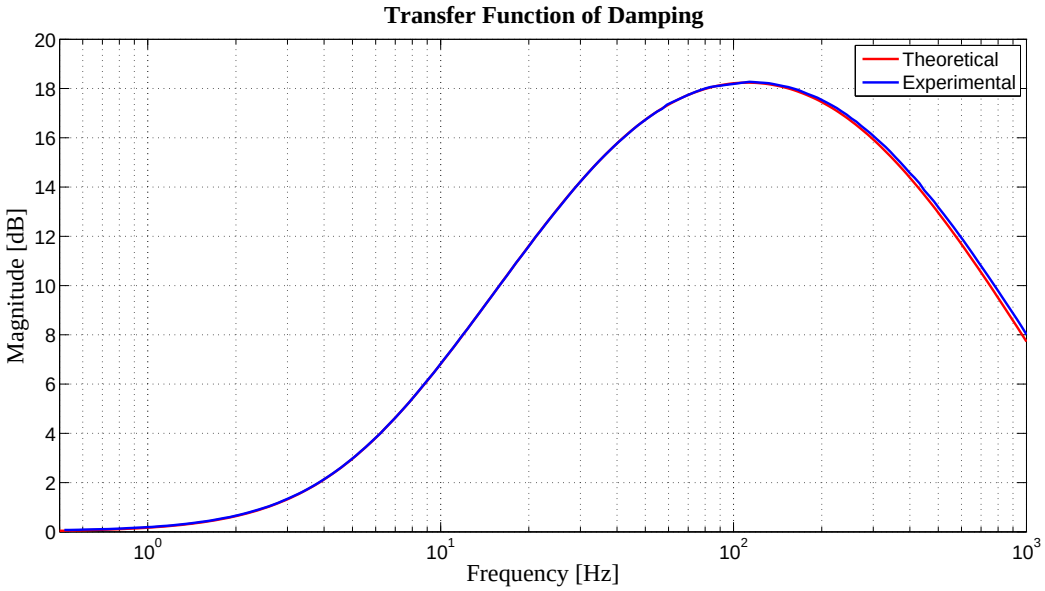

Figure 6: The transfer function of our high pass filter, as measured by our spectrum analyzer.

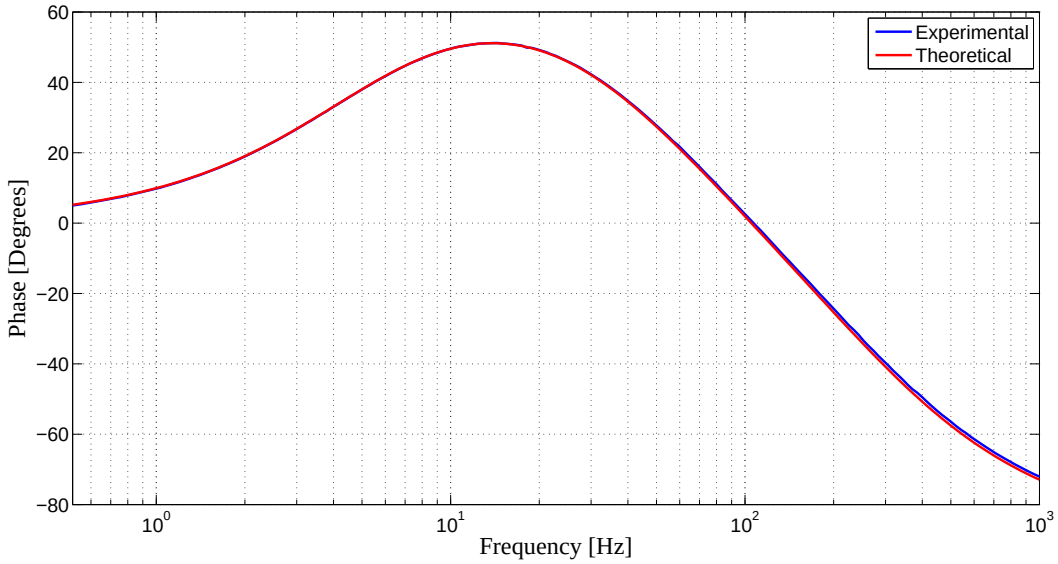

Figure 7: The phase of the high pass filter configuration, as recorded by the spectrum analyzer.

It was confirmed that the sensing PCB boards work as designed by measuring their transfer function with a spectrum analyser (see Fig. 6 and 7).

During calibration and testing of our setup, the HE sensors output signal was found to be very small. To boost the output of the HE sensors, an operational amplifier OP27 with two resistors (R1 = 1kΩ, R2 = 91kΩ), one capacitor(C1 = 8.5nF), and an effective gain of 91 were used. After moving the sensor closer to the plate, however, the gain was later on reduced to 11 (R1 = 1kΩ, R2 = 11kΩ) to avoid saturation of the ADC.

3.2.4 Optical Lever Sensors

Unfortunately, as explained by Miao et al, the Hall-effect sensors reading is affected by the magnetic field of the suspended magnets and, also, by the current through the actuator coils.[1] Sensing is in this way misleadingly coupled and can prohibit precise applications. For this reason, once successfully locking the system, we will also plan to replace our Hall-effect sensors with optical level ones. Optical level sensors detect laser bounced off the corner reflectors attached to the levitating plate. The reflected light is then sensed by a quad photodiode (QPD) which estimates the position of the plant. For a more elaborate description of optical level sensors, one can refer to Bhatt's work.[3]

3.3 ADC

The analog signal is sent to an ADC and sent to the computer. For our ADC, 20V produce $2^{16} = 65536$ bits, such that 1mV corresponds roughly to 3.3bits. However, the ADC interprets the signal as the voltage difference between a positive and negative source (for example, a 10V signal is interpreted as a signal from a +5V and -5V source) and the bits of the digital signal are only half (20 V correspond to $\frac{2^{16}}{2}$ what one would expect. That means the relationship between analog and digital signal for our ADC is

$$1\mathrm{V} = 2^{15}/20 = 1638\mathrm{bits}$$

3.4 Digital Feedback Filter

3.4.1 Transfer function of the system

With the use of the softwares medm and foton, digital feedback is used to adjust the transfer function of the levitating plate and stabilize its motion. For accurate feedback filtering, the transfer function of the plate needs to be known—at least approximately.. The configuration is unstable and can be modelled as a negative spring. For a single, linear degree of freedom, we model the motion of the levitated plate to be

$$\mathrm{m}\ddot{\mathrm{x}} = \mathrm{kx} - \mathrm{m}\gamma\dot{\mathrm{x}} = \mathrm{F},$$

or

$$\mathrm{m}(\ddot{\mathrm{x}} + \gamma\dot{\mathrm{x}} - \omega_{\mathrm{r}}^2\mathrm{x}) = 0,$$

where γ is the damping factor (due to, for example, air friction) and ω_{r} the resonance frequency of the plate. In the presence of external input forces, we can model the plate's motion with

$$\mathrm{m}(\ddot{\mathrm{x}} + \gamma\dot{\mathrm{x}} - \omega_{\mathrm{r}}^2\mathrm{x}) = \mathrm{F}_{\mathrm{tot}},$$

where $\mathrm{F}_{\mathrm{tot}}$ is the effective force acting on the plate. The total force can be further distributed to its components and consider two types of input disturbances:physical forces and feedback force, $\mathrm{F}_{\mathrm{FDB}}$, which we control. In our case, we are primarily keen on isolating the seismic noise, so we can ignore all physical forces but the ground motion. The plate's motion can then be simulated for a single, linear degree of freedom as

$$\mathrm{m}(\ddot{\mathrm{x}} + \gamma\dot{\mathrm{x}} - \omega_{\mathrm{r}}^2\mathrm{x}) = \mathrm{F}_{\mathrm{GND}} + \mathrm{F}_{\mathrm{FDB}}. \tag{12}$$

After a Laplace Transform, eq.12 becomes

$$\mathrm{mX(s)(s^2 + \gamma s - \omega_r^2) = F_{GND}(s) - G(s)X(s)},$$

where $\mathrm{F_{GND}}$ is the input force of the ground, associated with the ground's displacement—$\mathrm{X_{input}(s)}$—, G(s) is the applied feedback filter, and X(s) is the output, linear displacement of the plate. The transfer function of the system is therefore described by

$$\frac{\text{output}}{\text{input}} = \frac{\mathrm{X(s)}}{\mathrm{F_{GND}(s)}} = \frac{1}{\mathrm{m(s^2 + \gamma s - \omega_r^2) + G(s)}}. \tag{13}$$

The transfer function for angular degrees of freedom is derived in a similar way. The force equation is

$$\kappa\theta - \eta\dot{\theta} = \mathrm{I}\ddot{\theta} = \tau,$$

where τ is torque, κ is the torsional constant, η the damping coefficient, and I the moment of inertia corresponding to the specific angular degree. Rearranging the equation and including the input forces gives

$$\mathrm{I}\ddot{\theta} + \eta\dot{\theta} - \kappa\theta = \tau_{\mathrm{FED}} + \tau_{\mathrm{GND}}, \tag{14}$$

where τ_{GND} comes from the tilt of the ground. The transfer function for an angular degree of freedom is then obtained with a Laplace transform:

$$\frac{\Theta(\mathrm{s})}{\tau_{\mathrm{GND}}(\mathrm{s})} = \frac{1}{\mathrm{Is^2} + \eta\mathrm{s} - \kappa + \mathrm{G(s)}}. \tag{15}$$

However, the transfer function of the whole configuration changes if feedback control is

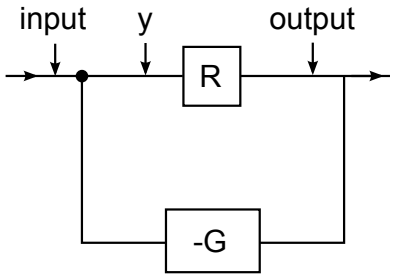

Figure 8: The diagram shows a simplified feedback loop, used in the maglev project.

applied. For a simplified setup, as the one shown in the block diagram,

$$\mathrm{O = Ry}, \tag{16}$$

where O is the output, and

$$\mathrm{y = I + F},$$

where G is the transfer function of the feedback, I the input, and F the feedback. It is also true that

$$\mathrm{F = -GO = -GRy}.$$

Then,

$$\mathrm{y = I - GRy}.$$

Solving for y gives

$$y = \frac{I}{1 + GR}. \tag{17}$$

Combining 16 and 17, the transfer function becomes

$$\frac{O}{I} = \frac{R}{1 + RG} = \frac{1}{R^{-1} - G} \tag{18}$$

Evidently, feedback control changes the behavior of the system. Since the feedback filter is designed with a computer, arbitrary control can be used to modify the transfer function of the whole system to correct the instability due to the negative spring term in all six degrees of freedom. There follows a more detailed description of the digital feedback form.

3.4.2 Design of Feedback Filter

Needless to say, the output displacement of the plate—effectively its transfer function—needs to be small for stable levitation. Even without knowing the exact shape of the transfer function, the system is inherently sensitive to disturbances associated with certain frequencies: near the low spectrum and near the resonance frequency.

Integrator In the absence of feedback control and in the low-frequency regime, where s≈ 0, the transfer function of the system becomes

$$\frac{X_{output}}{X_{input}} = \frac{1}{-m\omega_n^2},$$

for the linear degrees of freedom—where ω_n is the angular natural frequency—and

$$\frac{\Theta(s)}{\tau_{GND}(s)} = \frac{1}{-\kappa},$$

for an angular one. The resonance frequency of the magnetic levitation setup is presumably low, effecting a large output displacement. To counter this effect, we introduce an integrator factor, proportional to $\frac{1}{s}$, with our feedback filter to minimize the transfer function near the low-end of the frequency spectrum. Specifically, we designed the following transfer function with one zero and one pole for our feedback:

$$\frac{s + \omega_n}{s + 0},$$

where $\omega_n = 2\pi f_n$. In fig.9 one can see the theoretical prediction for the applied integrator.

Damping Similarly, at the resonance frequency

$$s^2 = -\omega_n^2$$

and the transfer function becomes

$$\frac{X_{output}}{X_{input}} = \frac{1}{m\gamma s}.$$

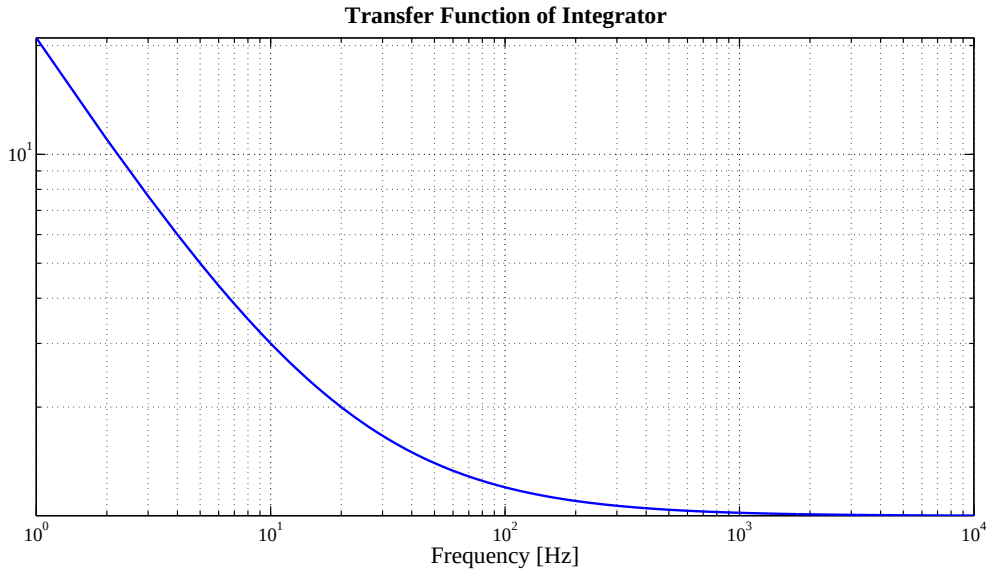

Figure 9: The transfer function of the integrator part of the feedback filter.

The damping factor is yet unknown, but can be assumed to be low since the maglev configuration—if successful—will be used inside a vacuum chamber. To prevent another peak in the transfer function, we introduce an extra damping term, proportional to s, in our feedback filter near the resonance frequency. To achieve this, we design the following transfer function

$$\frac{s + \omega_n}{(s + P_1)(s + P_2)},$$

where $P_1 = 40\pi \text{rad/s}, P_2 = 400\pi \text{rad/s}, \text{and} \omega_n \approx 10\pi$. There is also a DC part used to compensate the negative spring and make the plate stable. The compiled transfer functions of the integrator and damping parts are shown in Fig.10.

3.5 DAC

After the digital feedback filter and before the signal conditioning boards, the feedback signal is converted to analog form. For the DAC we used, the relationship between bits and mV was found to be

$$1\text{mV} = 3.3\text{bits}.$$

The connections between the DAC and the signal conditioning boards carry the signal and ground. However, it was wrongly believed that the wires carried positive and negative signal. Upon realizing the actuation conditioning boards did not respond to the digital feedback output, it was overseen that the positive signal was by mistake connected to the ground (and vice versa) and believed the problem was connecting the negative voltage output to the ground, which could drive current back to the DAC. More precisely, the DAC is not able to provide a large current (positive or negative). That is why the plant should have a large input impedance. To tackle this self-inflicted issue, a voltage follower was placed in the circuit before the dewhitening filter. Using four identical resistors(50kΩ), the output of

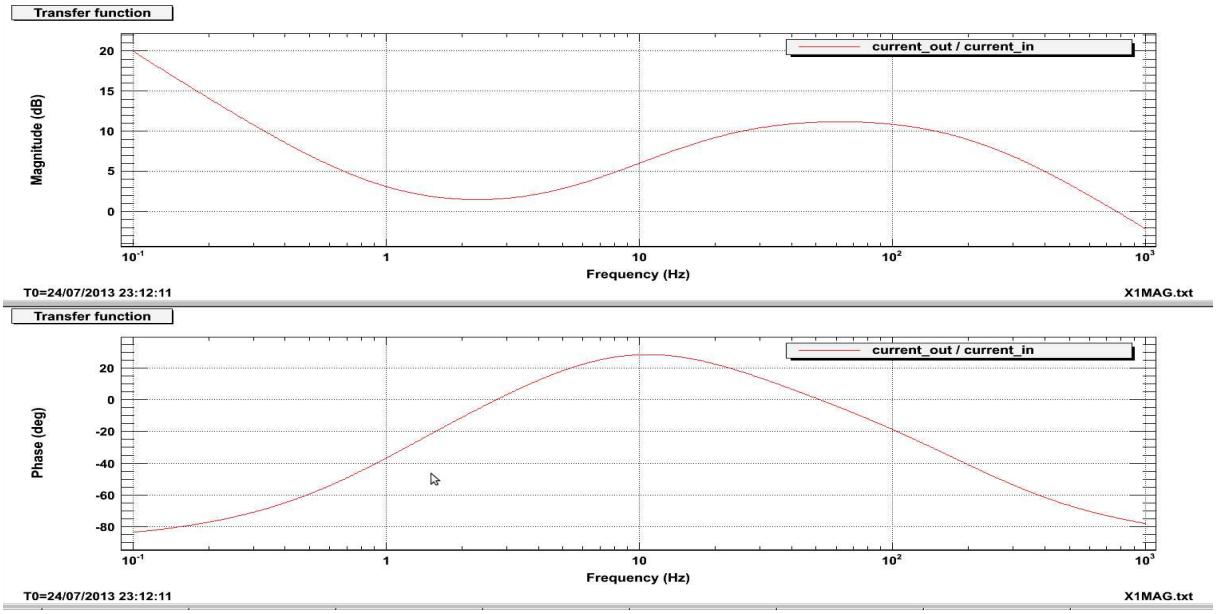

Figure 10: The picture is a screenshot of the Bode Plot of the applied feedback filter

.

the differential amplifier is the difference between the input signals. This circuit formation solves the problem;both the actual (misconnection) and the hypothetical one.

3.6 Actuators

After processing on a computer, we apply signal conditioning to 6 Coil-boards and 3 DC-offset ones. The Coil-boards drive current—depending on the feedback control—through, while the DC-offset boards are used for DC magnetic field offset, in addition to the constant magnetic field of the fixed magnets. The applied signal conditioning consists of a dewhitening filter and a current booster.

3.6.1 De-Whitening

The sensors' signal is at first modified via a high-pass filter configuration. To send the signal to the actuators in order to correct for the plate's displacements we have to first undo the whitening effect by introducing a low-pass filter. For ideal de-whitening, the cut-off frequencies must be the same, especially for the two lowest values (5Hz, 50Hz).To do so, we used the same configuration as in our high-pass filter case (see Fig. 5) whose transfer function is already known. We realize that $Z_0 < P_0$, so it has to be that P1 marks the lowest cut-off value if we are to have low-pass filtering. For unity gain at low frequencies, $R_1 = R_3$. Further constrained by our expectations for the poles and zero, we solve numerically for our circuit parameters: $\mathrm{R}_1, \mathrm{R}_2, \mathrm{R}_3, \mathrm{C}_1, \mathrm{C}_2$. In the end, we built a circuit, such that $\mathrm{P}_1 \approx 5$Hz, $\mathrm{Z}_0 \approx 52$Hz, and $\mathrm{P}_\mathrm{O} \approx 260$ with the following parameters:

$$\mathrm{R}_1 = \mathrm{R}_3 = 14.3\mathrm{k}\Omega, \mathrm{R}_2 = 4\mathrm{k}\Omega, \mathrm{C}_1 = 180\mathrm{nF}, \mathrm{C}_2 = 2.2\mu\ \mathrm{F}$$

Then, the calculated transfer function is

$$\frac{V'_{out}}{V'_{in}} \approx |-145\frac{s+303.58}{(s+32)(s+1389)}| \tag{19}$$

The measured transfer function and phase of our de-whitening circuit are shown in Figures 11 and 12.

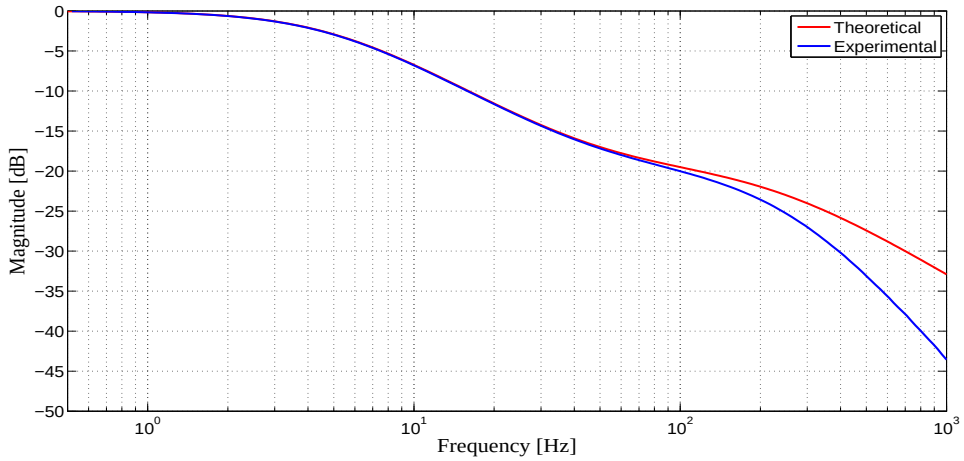

Figure 11: The Transfer Function of our Low-Pass filter configuration, as measured from the SR785 Spectrum Analyzer.

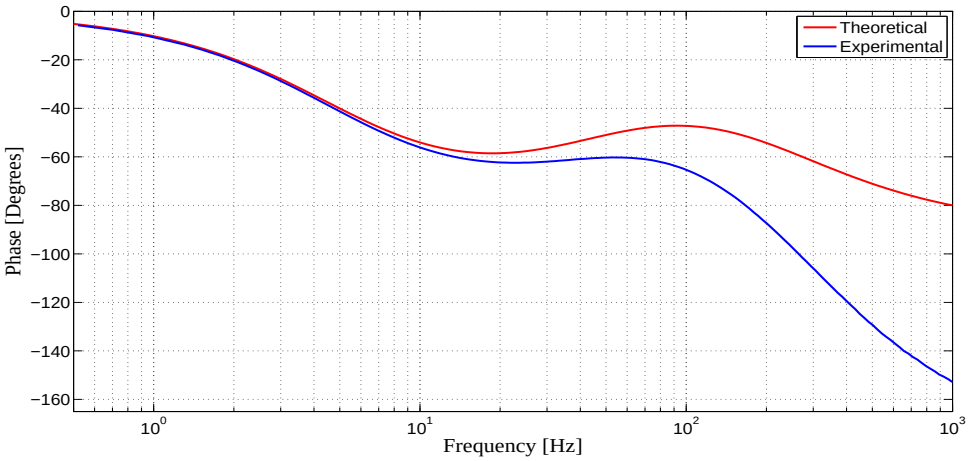

Figure 12: The phase of our low-pass filter configuration, as measured from the SR785 Spectrum Analyzer.

3.6.2 Current Boost

The OP27G op-amp, however, can only provide up to 10mA current, so the dewhitening circuit alone cannot drive enough current through the wires. To boost the current, we used

a current buffer (BUF634P) which can drive up to 250mA. The buffer itself is very noisy and we used it in a feedback loop with a low-noise op-amp (OP27GS).In the end, our actuator PCB boards include two circuits: one for low-pass filtering and one for current amplification.

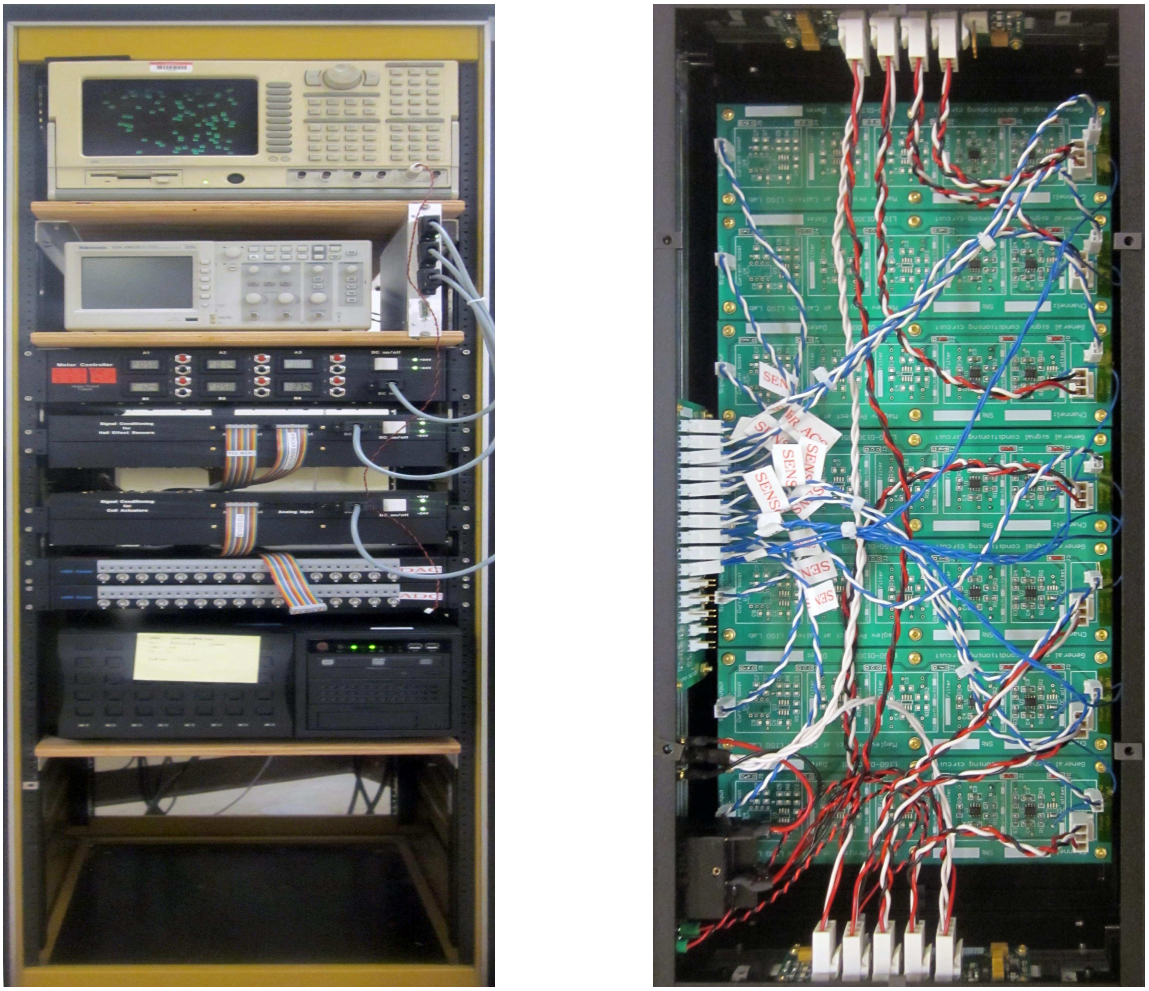

Figure 13: On the left, the chassis with the spectrum analyzer, oscilloscope and the motors (missing), sensors (missing), actuation, ADC, DAC boxes and the computer. On the left, the inside of the HE sensors box.

3.7 Simulation

Once the set-up of the experiment was ready, MATLAB Simulink was used to simulate the behavior of the system. In this way, the software predicts whether the configuration is stable and foretells the success of the experiment. It also provides insight to unknown parameters of the system—such as the appropriate gain, feedback control design, etc.—by allowing the user to tweak these values until achieving the desired performance. There follows a more detailed presentation of the MATLAB Simulink simulation of the maglev project.

The main interface of the magnetic levitation simulation is presented in Fig. 14 for 6 DoF. Given certain input variables, the software simulates the behavior of the system. Some of

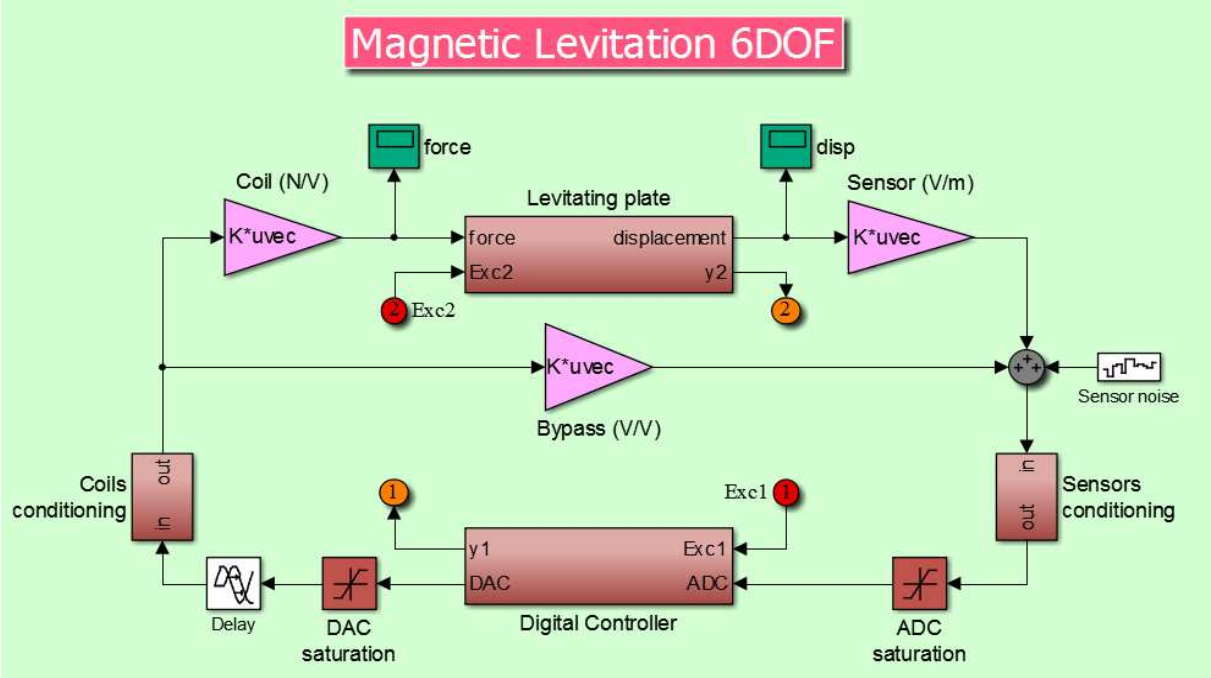

Figure 14: The main interface of our configuration in MATLAB Simulink for 6 degrees of freedom. The arrows and lines help the user follow the flow of action.

these variables refer to the specifics of our setup and are known; magnet mass, transfer functions of conditioning circuits, noise strength. Some other parameters, however, such as the correspondence between the volts sent to the actuators and the actual force acting on the plate, or the relationship between the displacement of the plate and the volts in the HE signal have been calibrated. Although these values are not very precise, MATLAB Simulink enables their refinement through comparison with the experimental outputs. In trying to find these unknown variables, their relationship is assumed to be linear near the equilibrium of the plate. Simulink needs to know -among others- how much force is applied on the plate given a certain actuation signal. To translate the signal to the force, the software needs a N/V (Newtons per Volts) relationship. This ratio was experimentally calculated to be around 0.002N/V. Similarly, the conversion factor between the displacement of the plant and the signal of the HE sensors was found to be around 100V/m.

Once the conversion factors were known, Simulink was used to produce the Bode plot of the system, as well as a response to a pulse, including ongoing background noise. Fig. 15 and 16 illustrate an example of theoretical stability achieved through Simulink. The peak at the Bode Plot reveals a resonance frequency around 0.2Hz in the z-direction. Similar was the behavior of the system for the rotations around the x- and y- axes, named roll and pitch respectively. At this point, the stability in the x-y plane was believed to be easily achieved with damping and were thus overlooked. As a result, stability was theoretically achieved for all 6 DoF. Despite this phenomenal success, at the beginning the plate failed to levitate in practice. After investigation, it was understood that the experiment failed for various reasons that are presented next.

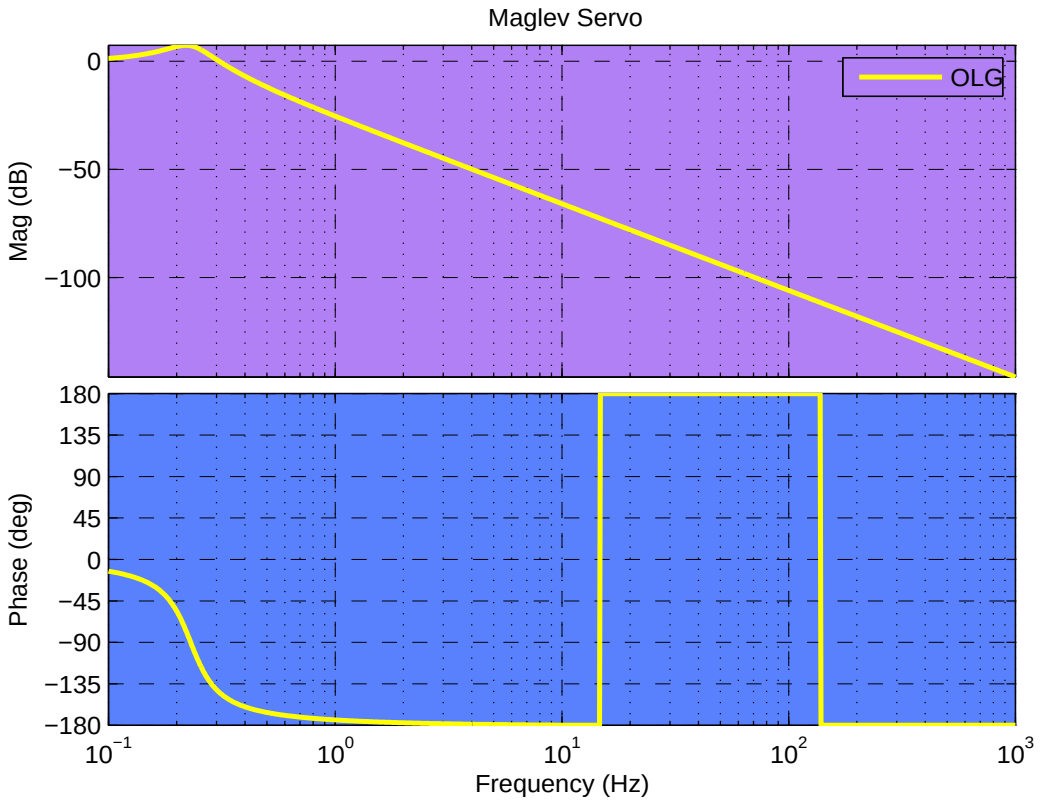

Figure 15: The Bode Plot of the plate in the z- (vertical) direction, where output is its displacement and input is the actuation force on the plate.

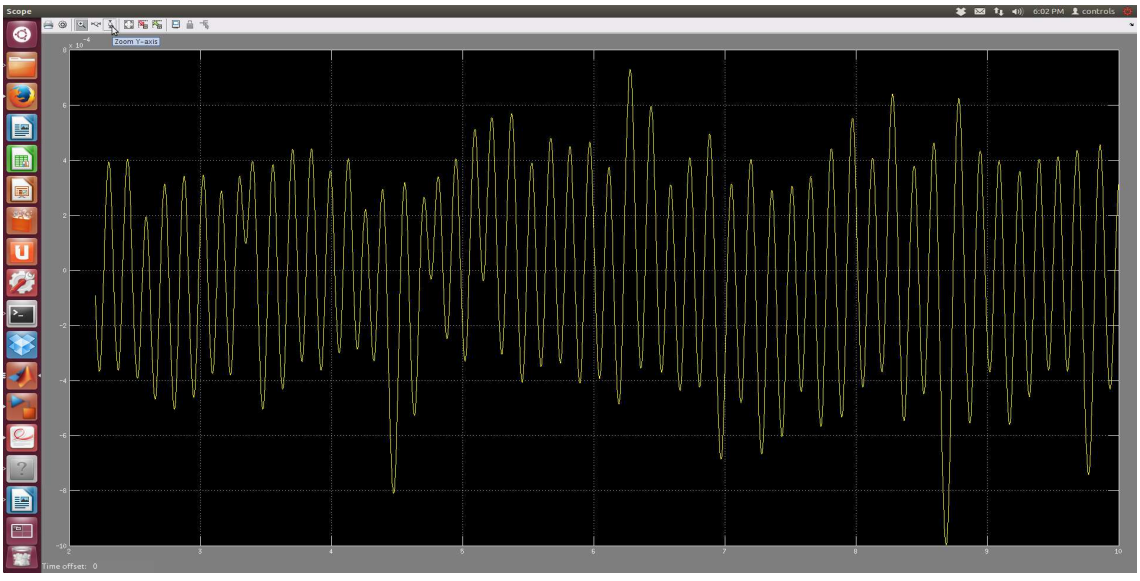

Figure 16: The graph shows the response of the setup to a triggered pulse of 20mV and HE sensor noise of roughly 1mV peak to peak. In this image of the simulation, the displacement of the plate in the z-direction never exceeds 800μm.

3.8 Levitation Issues and Solutions

3.8.1 Coupling effects

One of the issues that obstructed levitation was the cross coupling between coils and HE sensors. As fore-mentioned, the actuation force is in the form of current, which—flowing through the coils—provides an extra magnetic field. Ideally, the actuation force would only act on the plate to bring it back to equilibrium. However, the magnetic field created by the coils not only affects the plate, but is also sensed by the HE sensors directly. In this way, the readout of the sensors does not correspond solely to the displacement of the plate, but its signal is confounded with the extraneous effect of the actuation coils. To make matters worse, the signal of a single HE sensor suffers from cross-coupling, too; that is, it carries in it the effect of multiple actuation coils. Ideally, the actuation force would only locally affect the plate at the place opposite to the coil. This local displacement would—again ideally—be sensed only by one sensor, thus creating a pair of coils-sensors responsible for certain degrees of freedom for the plant's movement. In reality, however, the magnetic field created by the coils is strong enough to affect other surrounding HE sensors as well. Therefore, to clean the HE sensors' signal, the effect of the surrounding actuation coils has to be extracted from the sensors' output. Luckily, this can be adequately achieved within the feedback control.

The idea behind canceling the coupling effects inside the feedback filter lies in the fact that the actuation signal is always known. Could its effects on the HE sensors be somehow modelled, the part of the HE sensors output that is caused from the actuation signal could be precisely known and overlooked (subtracted digitally). The schematics in Fig.17 can help better simplify this idea.

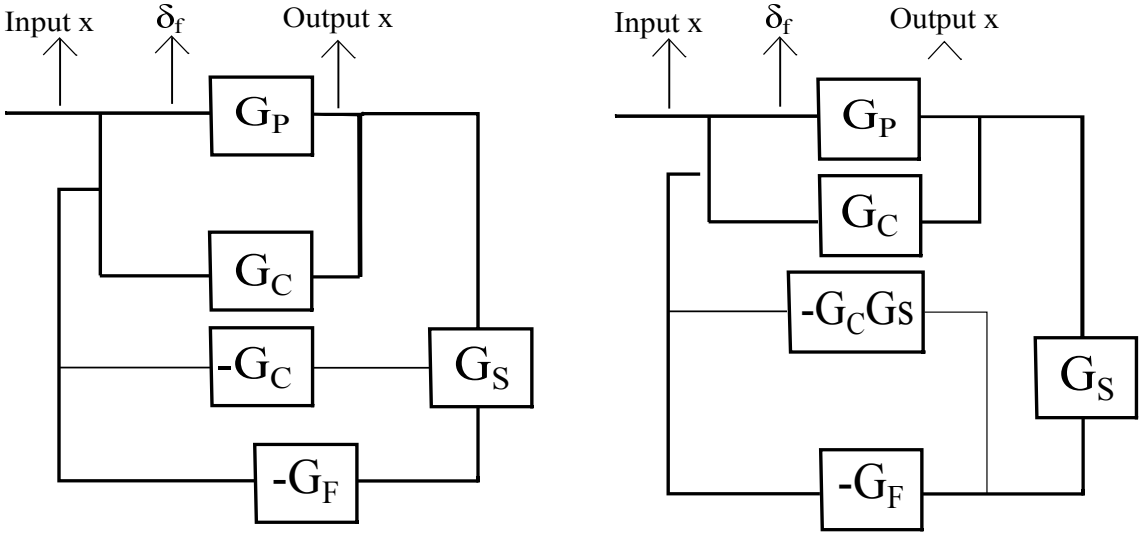

Figure 17: The above flow chart graphically presents the method of cancelling the coupling effects. The right figure is an equivalent, simplified version that shows how cancelation can occur inside the feedback control.

The transfer functions of the plant, the sensors, and the feedback control are represented by G_P, G_S, G_F, respectively. Provided that it too can be modelled, the transfer function of the coupling effect is represented with G_C. This extra loop that shows the coupling is

undesired but, in theory, could be subtracted from the system. The extra loop with the -G_C transfer function serves exactly this purpose. Of course, there is no way to prevent the sensors from reading the ambient magnetic field from the actuation signal. Then, the coupling cancelation must occur inside the digital feedback. If there is a way to expect and always know how much of the HE output is due to coupling, the signal can be cleaned. In practise, the difficulty lies in modeling the transfer function of the coupling over the whole frequency spectrum. Needless to say, a linear fit from manual measurements is in this case not enough.
Obtaining the transfer function of the coupling can itself be easily derived. Signal over a frequency spectrum is sent from the feedback filter (input) and the output of the sensors is, after the ADC, the input to the digital filter (output). The ratio $\frac{\text{output}}{\text{input}}$ over a frequency range then yields the transfer function of the coupling between the actuation coils and the sensors. It is important that, during this measurement, the plate is present in the setup and stays fixed close to its equilibrium. Since the plate carries magnets inside it, it affects the magnetic field produced by the coils and also creates some on its own. Therefore, a more realistic measurement of the coupling effect that will resemble the real-time feedback control should take place in the presence of the plate. In addition, the plate must stay still such that the HE sensors signal only carries information on the coupling effect and not on the plant's displacement. To fix the plate, the DC motors were pressed against it.

Measuring the transfer function of the coupling is of no use, unless it is transformed into an algebraic expression that can be fed in the digital control. Only then can the feedback calculate the expected coupling effect, based on the actuation signal, and subtract it from the output of the HE sensors. To model the coupling effect, the method of vector fitting was used to obtain a fitting transfer function with zeros, poles, and gain that resembles the behavior of the coupling.[5] Briefly, Vector Fitting uses a guess function

$$\sigma(s) = \sum_{n=1}^{N} \frac{\tilde{c}_n}{s - \tilde{a}_n} + 1,$$

whose zeros are the poles of the fitting function

$$f(s) = \sum_{n=1}^{N} \frac{c_n}{s - a_n} + d + sh,$$

where c_n,$\tilde{c}_n$, a_n, and $\tilde{a}_n$ are constants. Therefore, finding the poles of the f (s) function is translated to the easier task of finding the zeros of the guess function $\sigma(s)$. By guessing the poles of the fitting transfer function, Vector Fitting then solves for linear coefficients and finds a linear least-squares fit. The user is allowed to select the number of iterations, as well as number of poles and zeros allowed in the fitting function. Fig.18 shows an example of the Vector Fitting process. Allocation of the zeros and poles continues for a selected number of iterations. The resulting transfer function simulates the behavior of the coupling effect satisfactorily. Once the model fit is subtracted inside the digital filter, the residual signal coupling effect will be as small as 10^{-4}. Fig. 19 offers a comparison between the data and the modeled equation. Significant deviation occurs only at high-frequencies, outside the range of interest for the maglev project. The modeled transfer function was subtracted inside the feedback. A comparison between the coupling signal before and after compensation is

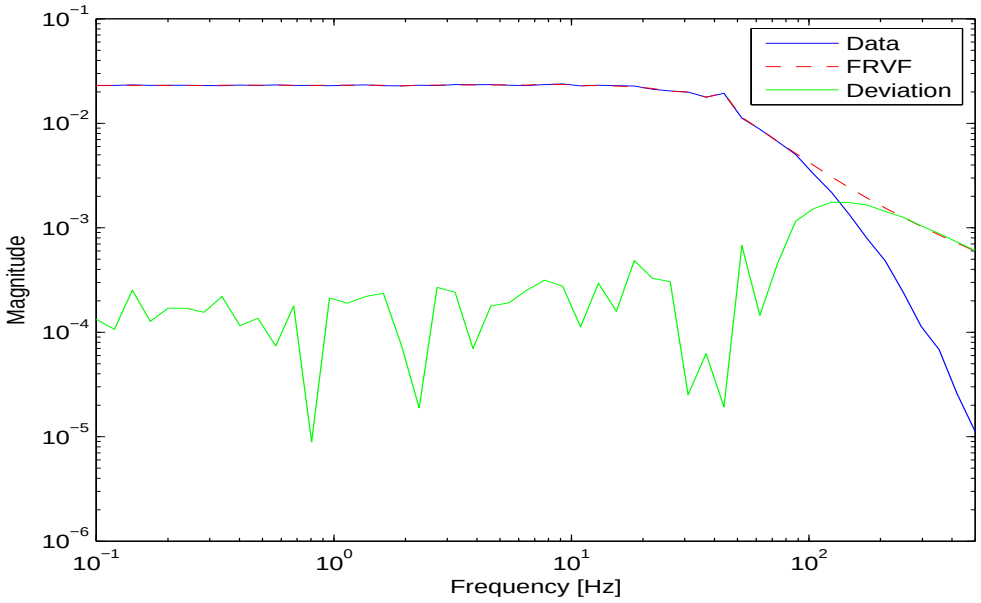

Figure 18: The diagram illustrates how the Vector Fitting method creates a transfer function to model the data. In the end, the created theoretical prediction matches the data down to 10^{-4} precision.

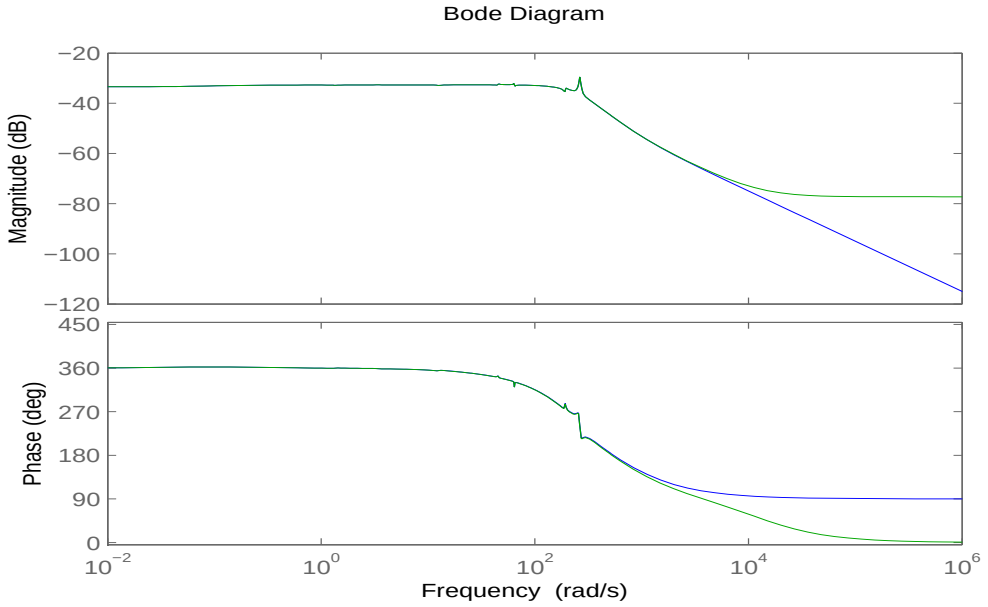

Figure 19: The figure is an estimation of the effect of ignoring high-frequency poles in the fitting. The blue curve is the one without the high-frequency poles.

offered in Fig. 20 and 21 and shows the effectiveness of the cancelation. The coupling effects of all AC sensors are shown to offer a feeling of how the relative weakness of cross-coupling from coils that lie further away.

Besides the Vector Fitting technique, mu metal was used to reduce the coupling effect.

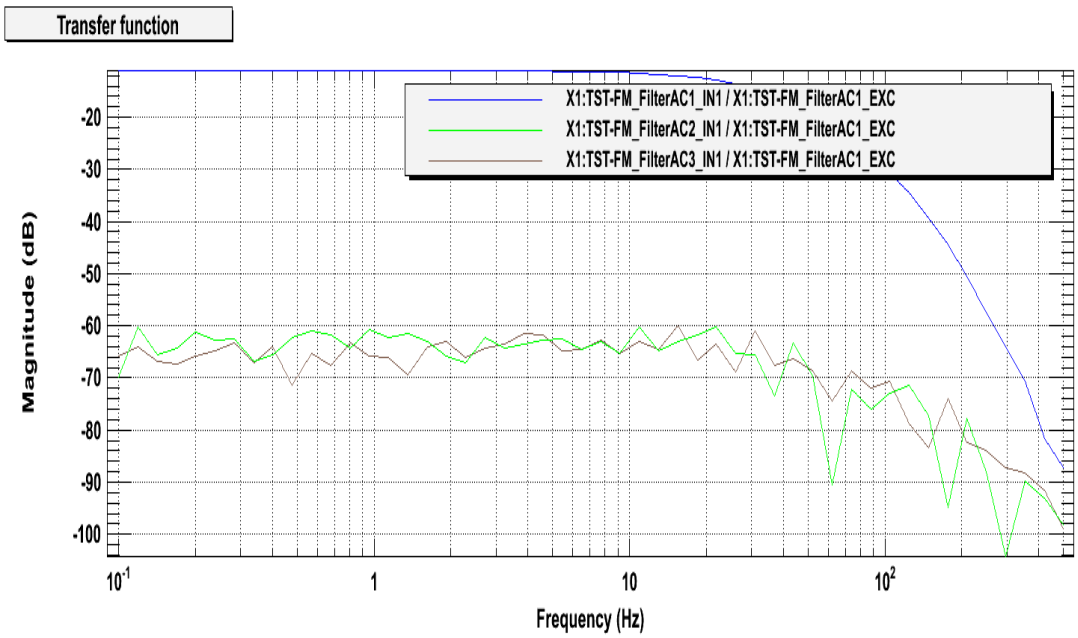

Figure 20
The figure is a printscreen of the Diagnostic Tools software. It shows the coupling signal between the AC1 coil and AC1 sensor before cancelation is of the order of -10dB.

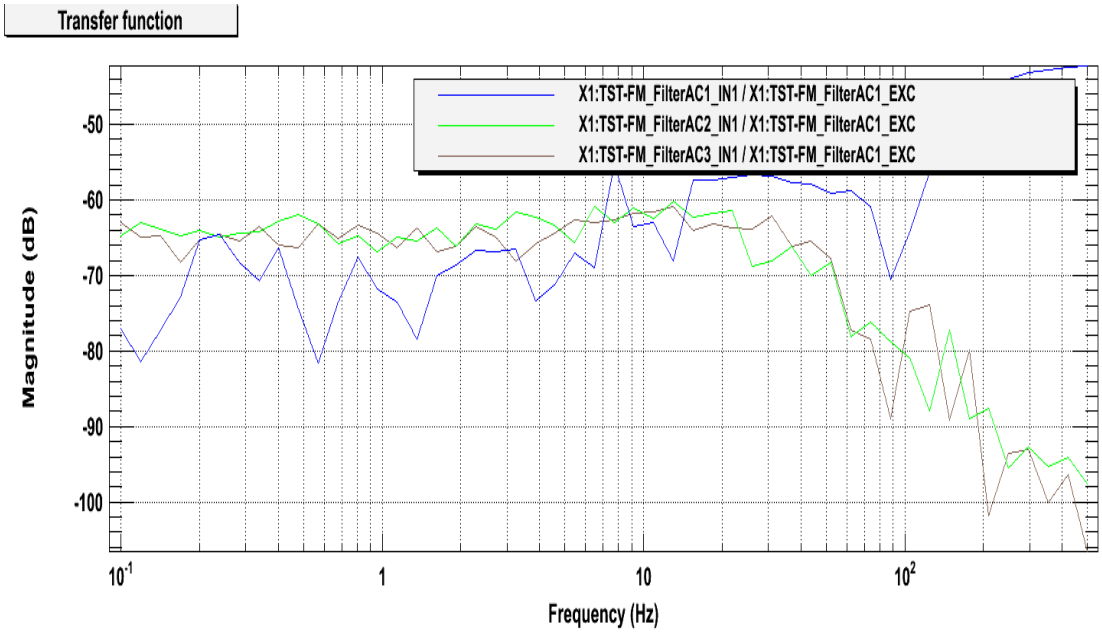

Figure 21: The figure is a printscreen of the Diagnostic Tools software. The coupling signal between the AC1 coil and AC1 sensor before cancelation is of the order of -70dB.

Mu-metal has high magnetic permeability and can so help shield the HE sensors from the magnetic field from the coils. Placing mu-metal around a single coil primarily protects its paired sensor against the magnetic field from neighboring coils or magnets of the plate that are further away. It should not interfere with the displacement's signal, since each HE sensor

is placed above a single magnet on the plate. The effectiveness of this technique is shown by comparing Fig. 22 and 23.

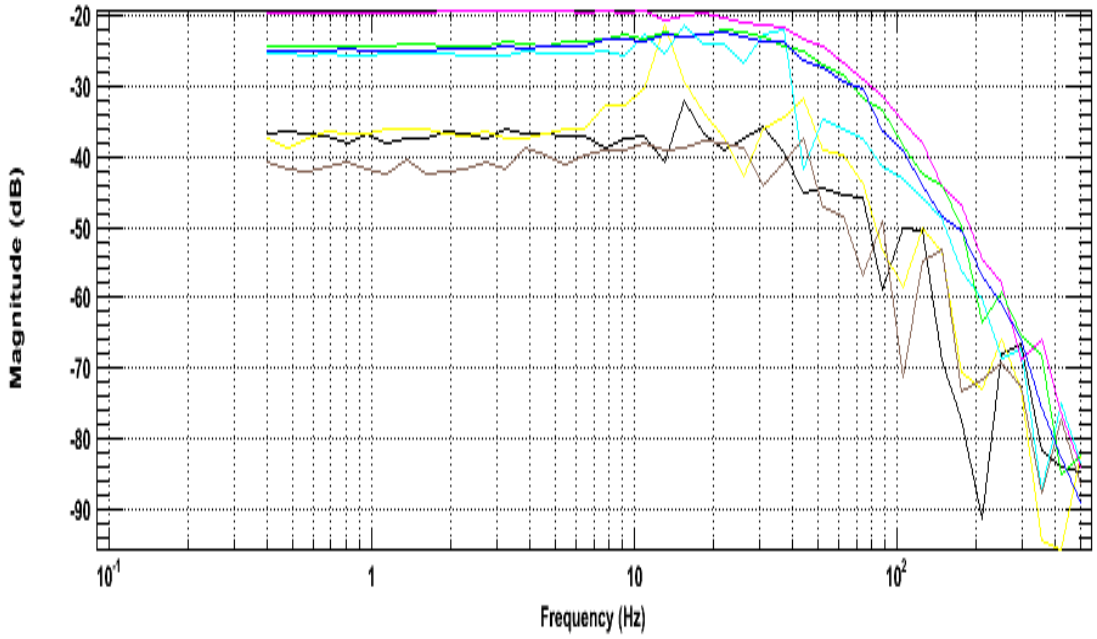

Figure 22: The figure is a printscreen of the Diagnostic Tools software. It shows the coupling signal in all HE sensors from a single coil before covering the HE sensors with mu metal.

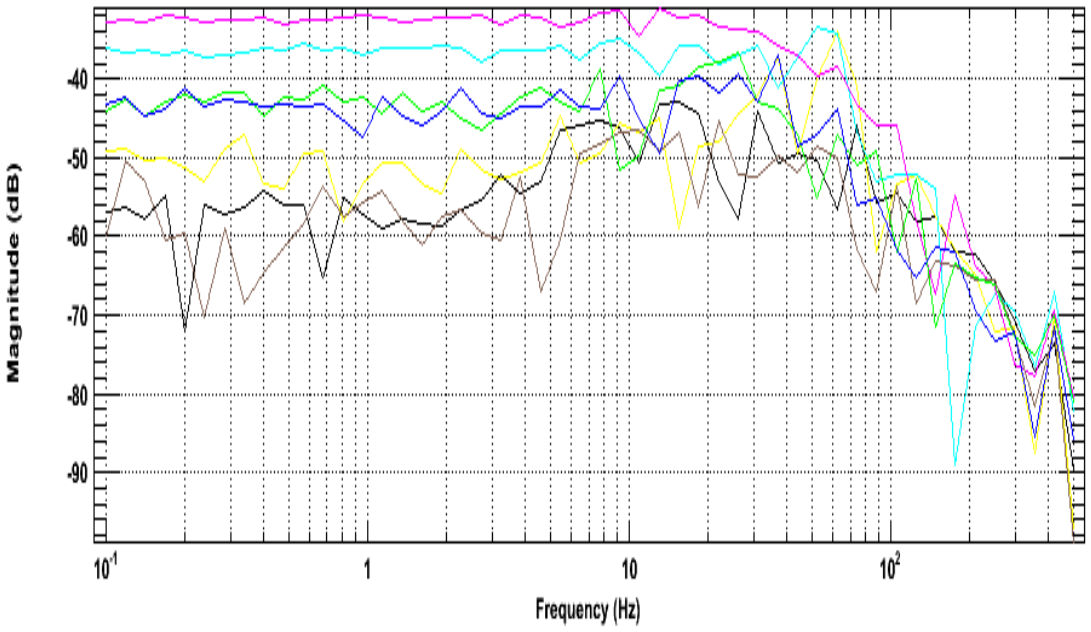

Figure 23: The cross coupling signals after the use of mu metal

3.8.2 Saturation

Another issue with levitation was the saturation of certain components of the circuit (ADC, DAC, and op-amps); they can provide up to 10V. This limitation necessitates a careful analysis of the gains in the system, such that the signal never exceed the allowed limit. Of course, the larger the displacement of the plate, the greater the produced signal and the gains may have to be sacrificed for a feedback control that will be effective over larger-scale displacements of the plate. In a sense, the purpose of balancing the gains serves to fully use the linear dynamical range of each part. In the case that this range is assumed to be 1mm, the gains were calculated in order to restrain the displacement of the plant below that value at all times; beyond that point the plate can presumably not be controlled. Fig. 24 shows

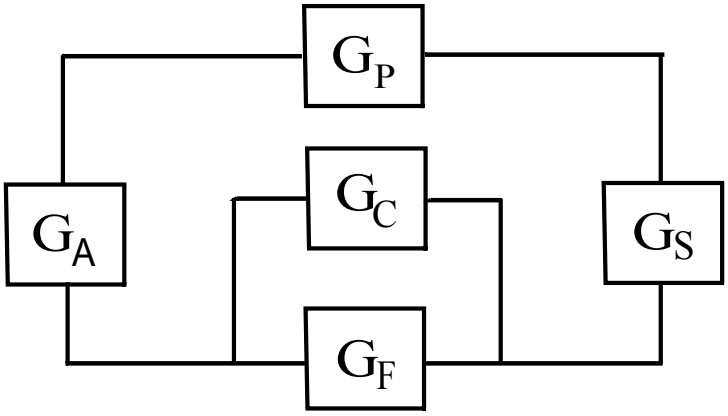

Figure 24: The flow chart shows the various components of the feedback control system and their corresponding gains/transfer functions.

the various gains and transfer functions of the feedback loop. To maintain the signal below saturation levels, one has to pay attention to the transfer function of the plate (G_P) and the coupling signal (G_C), as well as the gain of the sensors (G_S), the feedback, (G_F), and the actuation coils (G_A). Here is a more elaborate analysis. The first limitations to consider are the saturation levels of 10V at the output of sensors (due to the op-amp in conditioning circuit and then ADC), the output of the feedback (DAC), and also the output of the coils (op-amp limit). Given the gain of the coils ($G_A = 1$), if the signal is to remain below 10V after the coils conditioning board, the DAC output should also stay below

$$\mathrm{DAC}_{\mathrm{output}} \leq = 10\mathrm{V}.$$

After moving the HE sensors closer to the plant, the conversion between the displacement and the produced signal was ≈ 100 mV/mm. Therefore, a 1mm displacement of the plant results in 100mV in the HE sensors, which is amplified by the conditioning circuit's gain: $G_S = 11$. Therefore, were the plant to remain within 1mm from its equilibrium, it can produce up to 1100mV in the ADC. Noise also adds to the signal from the HE sensors, but its contribution was insignificant after reducing G_S to 11; it was measured to be less than 5mV peak to peak. The residual from the coupling signal after the cancelation in the feedback filter is at worst -40dB. With a maximum DAC output of 10V(while the gain of the actuation conditioning circuit was removed), that means that the residual coupling signal can be at most 4mV. Thus, the digital feedback receives

$$\mathrm{Displacement} + \mathrm{Noise} + \mathrm{Coupling} \leq 1.11\mathrm{V(peaktopeak)}.$$

Constrained by the DAC output, the maximum gain inside the feedback filter is well defined:

$$G_F = 10/1.11 \approx 9.$$

Apart from the coupling effects and the saturation issue, there are other parameters that affected levitation. The signal from the displacement of the plant was at first very weak. In fact, it was of the same order of magnitude as both the coupling signal and noise. Moving the HE sensors closer to the plate increased the signal significantly (about by a factor of 50) and solved the problem. The amplitude of noise was another problem, since it was initially about 40mV. Reducing the gain of the sensors conditioning board from 91 to 11 also reduced noise by a factor of 8.

4 Results and Future Work

Correcting the fore-mentioned problems allowed for the levitation of the plate. Stability in the horizontal degrees of freedom (x and y translations and yaw) is secured by enough damping. To achieve levitation, stability in the z-direction, as well as pitch and roll was necessary. Contrary to the initial thought, it was easier to achieve full lock of the system if dealing with all three vertical degrees of freedom simultaneously. That is because instability in one degree would tend to destabilize the whole setup. After experimenting with the appropriate feedback, the plate was successfully levitated, demonstrating successful sensing and control in 6DOF. To confirm the feasibility of the maglev approach, the isolation performance remains to be measured. Nonetheless, the original goal of the project was to achieve a low resonance system to be used for noise isolation. Besides the fundamental goal, there are ways to enhance the performance of the setup. Suggestions for future work are enumerated next.

1. The measurement of the transfer function of different parts. The most important one is the transfer function of the levitated plate, because it reveals the isolation performance of our setup.

2. Reduction of the resonance frequency. Tuning the magnetic field with the DC coils can bring the equilibrium point closer to the maximum of the magnetic force, which allows to achieve a lower rigidity. This step should be done recursively until the rigidity is as low as around 0.1Hz which is the target resonant frequency.

3. Use of optical level sensors for higher precision measurements of the displacement.

References

[1] Adhikari, R., Arai, K., and Miao, H., *Some basics for magnetic levitation*. Retrieved from http://www.ligo.caltech.edu(2013).

[2] Allegro MicroSystems, Inc., *Continuous-Time Ratiometric Linear Hall Effect Sensor ICs*. Retrieved from www.allegromicro.com.

[3] Bhatt, N.,*Characterization, Commissioning and Implementation of the Optical Lever System at Caltechs 40m Advanced LIGO Prototype Lab*. Laser Interferometer Gravitational Wave Observatory (LIGO) (2003)

[4] Abbott, R., Heefner, J., Osthelder, C., *Chassis Power Regulator PCB*. LIGO Document D1000217 (2010)

[5] Gustavsen, B., and Semlyen, A., *IEEE Transactions on Power Delivery*, **14 (1999), 1052-1061**